Engineering Structures 241 (2021) 112415

Contents lists available at ScienceDirect

Engineering Structures

journal homepage: www.elsevier.com/locate/engstruct

A redesigned approach to the additional damping method in the dynamic analysis of simply supported railway bridges

Bernhard Glatz *, Josef Fink

TU Wien, Institute of Structural Engineering, Karlsplatz 13, 1040 Vienna, Austria

ARTICLE INFO

Keywords:
Bridge dynamics
Additional damping
Vehicle-bridge interaction
Moving Load Model
Detailed Interaction Model

ABSTRACT

In the dynamic analysis of simply supported railway bridges, the choice of vehicle models directly affects the quality of computed results. Simple moving load models usually overestimate the bridge response in comparison with models taking into account vehicle-bridge interaction effects. In order to compensate for this discrepancy, the Eurocode allows the increasing of structural damping for analyses performed with a moving load model. The specified additional damping is based on investigations carried out by the European Rail Research Institute in 1999 and may yield non-conservative results.

This paper describes an extensive parametric study inspired by the common Additional Damping Method, aiming to eliminate its identified shortcomings. The applied input parameters for the study are based on existing European simply supported bridge structures with a ballast layer. In order to match the vertical accelerations computed with the Detailed Interaction Model, the additional damping for the Moving Load Model is determined for four European high-speed trains. The results show that the additional damping as integrated in the Eurocode is non-conservative. A redesigned approach enables the definition of conservative additional damping functions depending on the natural bridge frequency, the bridge mass and the train type.

1. Introduction

The dynamic behaviour of railway bridges under high-speed traffic has been investigated intensively by scientists and engineers in the recent years. It is especially the choice of calculation models of both the bridge structure and the crossing vehicles that proved to be a crucial factor in obtaining sufficient results for the given assignment.

Regarding the vehicle stage, the Moving Load Model (MLM) is used in numerous investigations of the dynamic behaviour of simply supported bridge structures [1–3] and it is established in the standardisation of dynamic analysis [4]. The MLM provides the highest degree of simplification by modelling the vehicles as a series of single loads F_i, which are moving over the bridge girder (Bernoulli-Euler beam with span L, bending stiffness EJ, mass per unit length μ, damping ζ) with constant velocity v (see Fig. 1). The coordinates x_i describe the position of the loads F_i ($i = 1,2,\ldots,m$) on the bridge.

The accuracy of the dynamic analysis can be enhanced by taking into account vehicle-bridge-interaction (VBI) effects, which – compared to the MLM – tend to reduce the dynamic bridge response at resonance [4]. In the Detailed Interaction Model (DIM), the vehicles are modelled as multi-degree-of-freedom systems moving over the bridge (see Figs. 2 and 3). The wheelsets (mass m_W) are connected to the bogies (mass m_b, moment of inertia J_b) through the primary suspension stage (stiffness k_p, damping coefficient c_p) and the bogies are connected to the car body (mass m_c, moment of inertia J_c) through the secondary suspension stage (stiffness k_s, damping coefficient c_s). For trains with the conventional configuration of two bogies per car body, the DIM is depicted in Fig. 2. For this train type, the vertical coupling of adjacent cars is neglected in the analysis model.

The DIM for trains with Jacobs bogies is shown in Fig. 3. In this train type, vertical displacements between adjacent cars are coupled.

If the DIM is applied in dynamic analyses, it is reasonable to distinguish between the bridge subsystem and the multi-body vehicle subsystem, which are coupled through time-dependent wheel-rail contact forces. It is assumed that the wheels stay in contact with the bridge at any time to disable a lift-off from the rails.

Various studies showed that the maximum vertical vibration of bridges can be reduced considerably by taking into account the VBI [5–9]. The evaluation parameter for these studies is the vertical bridge deck acceleration, as it becomes controlling in many cases for the

* Corresponding author.
E-mail addresses: bernhard.glatz@tuwien.ac.at (B. Glatz), josef.fink@tuwien.ac.at (J. Fink).

https://doi.org/10.1016/j.engstruct.2021.112415
Received 16 November 2020; Received in revised form 18 March 2021; Accepted 15 April 2021
Available online 5 May 2021
0141-0296/© 2021 The Authors. Published by Elsevier Ltd. This is an open access article under the CC BY license (http://creativecommons.org/licenses/by/4.0/).

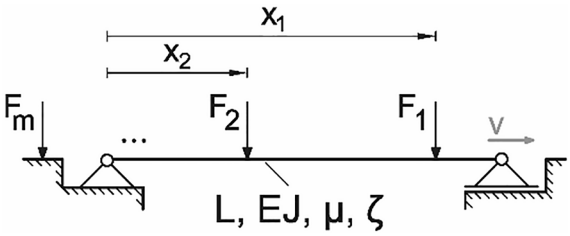

Fig. 1. Moving Load Model (MLM).

verification of the serviceability limit states of simply supported bridges. *Doménech et al.* [6] identified the ratio between natural bridge and bogie frequencies, the ratio between bridge and bogie masses and the ratio between bridge and car length as the main parameters for the influence of the VBI. The bogie frequency n_p is defined in [6] as

$$n_p = \frac{1}{2\pi}\sqrt{\frac{2k_p}{m_b}} \tag{1}$$

wherein k_p is the stiffness of the primary suspension stage and m_b is the mass of the bogie.

1.1. Additional damping method

The Additional Damping Method (ADM) is specified in the Eurocode [4] as an alternative to VBI analyses. Within the ADM, the positive VBI effects of reduced vertical vibration amplitudes are taken into account in MLM analyses by increasing the damping of the bridge structure. The extent of the additional damping $\Delta\zeta$ is specified as a function of the span L (Fig. 4).

The theoretical basis for the ADM was documented by the European Rail Research Institute (ERRI) in [10]. The additional damping was determined by increasing the bridge damping for MLM analyses until the vertical peak accelerations equalled the ones calculated with the Simplified Interaction Model (SIM, see Fig. 5). These comparisons between the MLM and the SIM were performed for a parametric field of simply supported bridges and the two train types ICE-2 and Eurostar. For all calculated values $\Delta\zeta$, a rational function (depicted in Fig. 4) was defined as a lower limit. The following assumptions were made for the SIM in [10]:

- The mass of the wheelsets and the oscillation of the car bodies masses are neglected.
- The oscillating mass m is defined as the half of the bogie mass m_b.
- The primary suspension stage is represented by the stiffness k and the damping coefficient c.

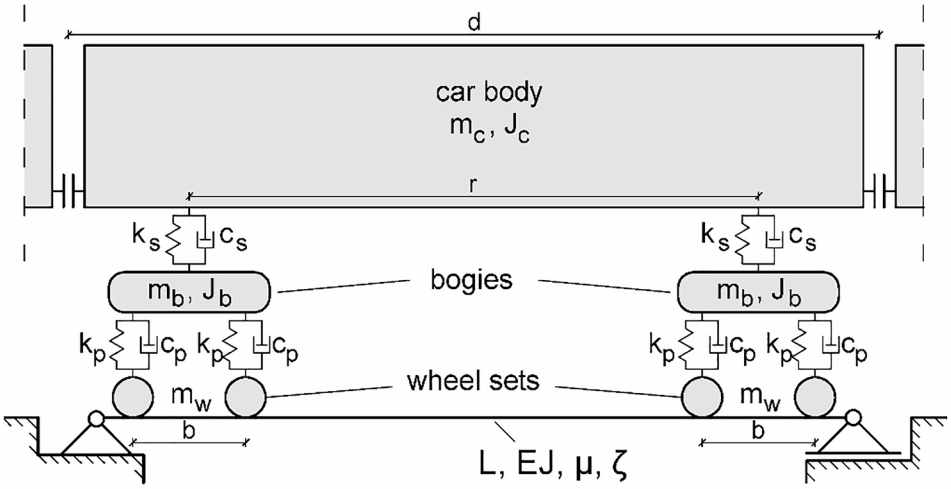

Fig. 2. Detailed Interaction Model of a conventional coach.

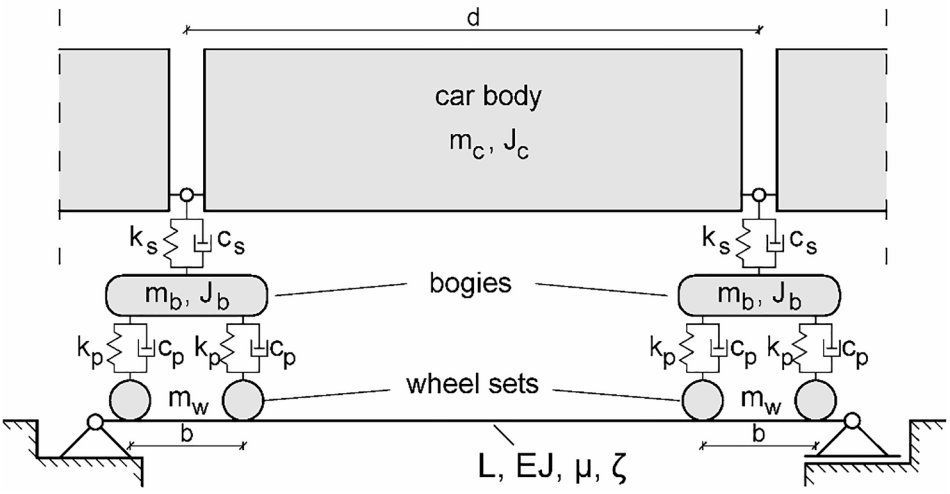

Fig. 3. Detailed Interaction Model of a coach with Jacobs bogies.

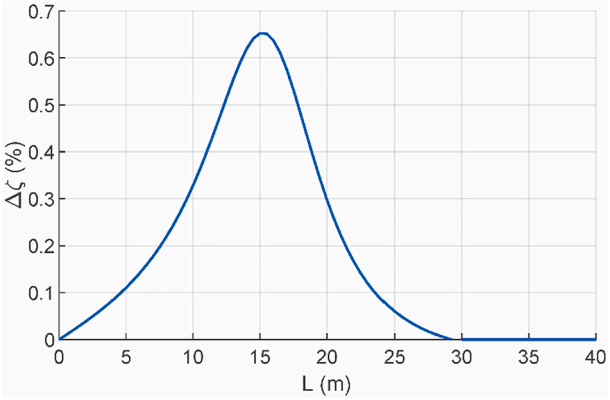

Fig. 4. Additional Damping $\Delta\zeta$ (%).

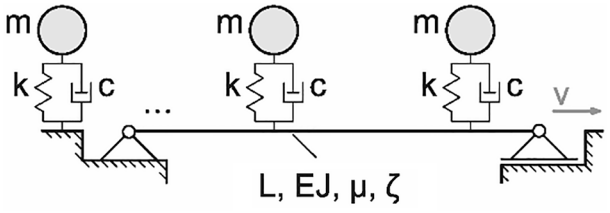

Fig. 5. Simplified Interaction Model [10]

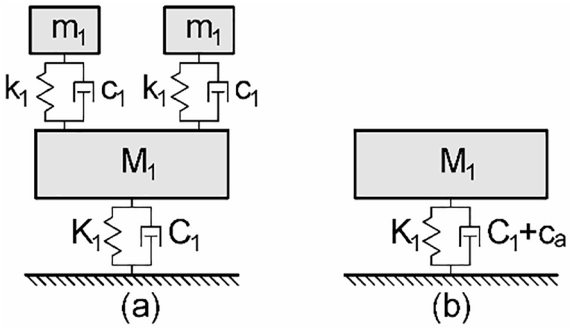

Fig. 6. Mathematical models for the coach-bridge coupling system; (a) simplified model with two tuning units; (b) equivalent model including additional damping c_a [12]

- The loads on the moving systems are assumed to be equal to the static axle loads.

Apart from the fact that, compared to the DIM, the SIM cannot cover all the interaction effects and therefore the calibration of $\Delta\zeta$ according to the DIM should be preferred, further shortcomings of the ADM are identified in [7,11]. Furthermore, it is shown in [8,11] that the additional damping given in the Eurocode can yield non-conservative results in particular cases.

1.2. Equivalent additional damping approach

Yau et al. [12] present the Equivalent Additional Damping Approach (EADA) that delivers an analytical formula for the determination of the additional damping for short span bridges and provides the physical background for additional damping methods. The EADA considers only the first vibration mode of a simply supported beam, which is represented by the modal mass M_1, the modal stiffness K_1 and the modal damping C_1 in a mathematical model (Fig. 6). For the vehicle modelling, it is assumed that two bogies of adjacent coaches are present on the bridge. The two tuning units in Fig. 6(a) represent the dynamic properties of a half coach, which are the modal mass m_1, the modal stiffness k_1 and the damping c_1. The damping ratio of the equivalent suspension system is denoted as [12]:

$$\zeta_1 = \frac{c_1}{2m_1\omega_1}; \quad \text{with} \quad \omega_1 = \sqrt{\frac{k_1}{m_1}} \tag{2}$$

The additional damping c_a for an equivalent model shown in Fig. 6 (b) is adjusted, so that the resonant amplitude of the main mass M_1 is equal in both systems (Fig. 6(a) and 6(b)).

As a result, the simplified formula for the additional damping ratio is given in [12]

$$\Delta\zeta_{EADA} \approx \mu_1 r_1 \sqrt{r_1^2 + (2\zeta_1)^2} \tag{3}$$

wherein $\mu_1 = m_1/M_1$ is the modal mass ratio, $r_1 = \omega_1/\Omega_1$ is the frequency ratio of the coach-bridge system and $\Omega_1 = \sqrt{K_1/M_1}$.

1.3. Aims of the study

This study aims to adjust the input parameters for the ADM in order to eliminate many shortcomings of the current method. Therefore, extensive dynamic analyses for parameterised simply supported bridges with different masses and four train types are carried out. The additional damping $\Delta\zeta$ to adjust the peak vertical acceleration calculated with the MLM to the corresponding value calculated with the DIM is determined for various bridge-train combinations. Displaying the resulting values of $\Delta\zeta$ as a function of the fundamental bridge frequencies enables the definition of conservative lower bounds of $\Delta\zeta$ for each train type. The presented method aims to yield more reliable additional damping values compared to the ADM without complicating the practical application.

2. Mathematical models

The equations of motion (EOM) for a train transit over a simply supported Bernoulli-Euler beam are widely described in literature. In order to formulate the given problem mathematically, this study uses a modal superposition approach for the bridge subsystem, which is documented in [5]. The EOM for the vehicles both of conventional trains and trains with Jacobs bogies are formulated by means of the principle of virtual displacements following the algorithm given in [13]. The following Sections 2.1 and 2.2 give a short overview of the applied mathematical models. The detailed derivations of the applied EOM are formulated in [14].

2.1. Bridge subsystem

In order to describe the dynamic behaviour of the bridge structure mathematically, the Bernoulli-Euler beam in Figs. 1–3 must be discretized. *Clough* and *Penzien* [15] introduce the lumped-mass procedure, the formulation of generalized displacements and the finite element concept as possible discretization methods. For this study, the method of generalized displacements is used by expressing the deflection shape $w(x,t)$ of the bridge as

$$w(x,t) = \sum_{j=1}^{n} q_j(t)\phi_j(x) \tag{4}$$

wherein x is the bridge coordinate, starting from the left support, t is the time, q_j are the generalized displacements, ϕ_j are the shape functions and n is the number of considered shape functions. By using the eigenfunctions of the simply supported Bernoulli-Euler beam as shape functions in Eq. (4), the modal equation for the bridge subsystem can be expressed as:

$$\boldsymbol{M\ddot{q}} + \boldsymbol{Z\dot{q}} + \boldsymbol{Kq} = \boldsymbol{P} \tag{5}$$

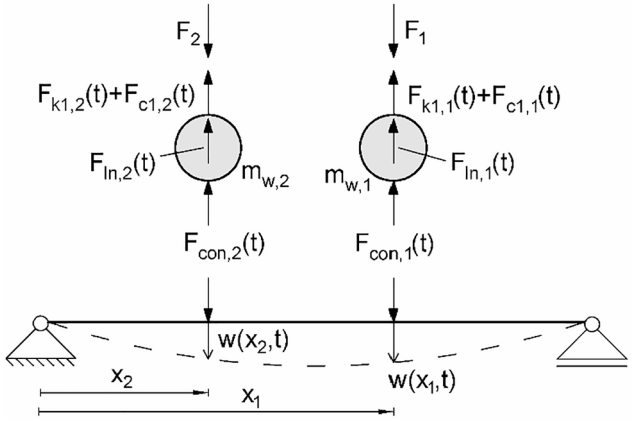

Fig. 7. Forces acting on the bridge and the wheelsets (DIM).

The left side of Eq. (5) contains the modal mass, damping and stiffness matrices $\boldsymbol{M}$, $\boldsymbol{Z}$ and $\boldsymbol{K}$ and the vectors of generalized displacements, velocities and accelerations $\boldsymbol{q}$, $\dot{\boldsymbol{q}}$ and $\ddot{\boldsymbol{q}}$. The damping matrix $\boldsymbol{Z}$ is composed using Rayleigh damping.

If the MLM is chosen as the vehicle model, the generalized load vector $\boldsymbol{P}$ in Eq. (5) can be written as

$$\boldsymbol{P} = \sum_{i=1}^{m} F_i \Gamma_i(x_i)\phi(x_i) \tag{6}$$

wherein F_i are the axle loads, m is the number of loads, x_i is the position of the load F_i on the bridge and $\phi(x_\mathrm{i})$ is the column vector of the mode shapes of the bridge. The rectangle function $\Gamma_\mathrm{i}(x_\mathrm{i})$ returns 1 for the loads present on the bridge at the regarded time-step and 0 for the remaining loads.

Within the DIM, the vehicles are represented as rigid bodies connected through linear spring and viscous damping elements. The spring and damping forces are defined positively for elongations in the suspension systems. As the dynamic forces acting on the wheelsets in Fig. 7 must always stay in balance with the static axle loads F_i, the dynamic equilibrium can be formulated as

$$F_i = F_{con,i}(t) + F_{k1,i}(t) + F_{c1,i}(t) + F_{In,i}(t) \tag{7}$$

wherein $F_{\mathrm{k1,i}}$ and $F_{\mathrm{c1,i}}$ are the primary spring and damper forces and $F_{\mathrm{con,i}}$ are the contact forces between the bridge and the wheelsets. The assumption of steady contact between the bridge and the wheelsets allows the inertial forces of the wheelsets $F_{\mathrm{in,i}}$ to be expressed as

$$F_{In,i}(t) = m_{w,i}\ddot{w}(x_i,t) \tag{8}$$

wherein $m_{\mathrm{w,i}}$ are the masses of the wheelsets and $\ddot{w}(x_\mathrm{i},t)$ are the vertical bridge accelerations at positions x_i. Considering that the axle positions x_i are time-dependent, the vertical bridge accelerations at these positions can be written in generalized form as the second time derivatives of Eq. (4), as in [1,14]:

$$\ddot{w}(x_i,t) = \sum_{j=1}^{n}\left[\ddot{q}_j(t)\phi_j(x_i) + 2v\dot{q}_j(t)\phi_{j,x}(x_i) + v2q_j(t)\phi_{j,xx}(x_i)\right] \tag{9}$$

In Eq. (9), v is the vehicle speed, $\phi_{\mathrm{j,x}}$ and $\phi_{\mathrm{j,xx}}$ are the first and the second derivatives of the mode shapes with respect to x.

The bridge load vector $\boldsymbol{P}$ is modified for the DIM by substituting the axle loads F_i in Eq. (6) with the contact forces $F_{\mathrm{con,i}}$. Considering this modification and Eqs. (5), (7), (8) and (9), the EOM of the bridge subsystem for the DIM can be written as:

$$\boldsymbol{M}\ddot{\boldsymbol{q}} + \boldsymbol{Z}\dot{\boldsymbol{q}} + \boldsymbol{K}\boldsymbol{q} = \sum_{i=1}^{m}\{F_i - F_{k1,i}(t) - F_{c1,i}(t) - m_{w,i}\left[\phi(x_i)\ddot{\boldsymbol{q}} + 2v\phi_{,x}(x_i)\dot{\boldsymbol{q}} + v2\phi_{,xx}(x)\boldsymbol{q}\right]\}\Gamma_i(x_i)\phi(x_i) \tag{10}$$

2.2. Vehicle subsystem

Additionally to the EOM for the bridge subsystem in Eq. (10), a second equation describes the motion of the vehicle masses in the DIM:

$$\boldsymbol{M}_V\ddot{\boldsymbol{u}} + \boldsymbol{Z}_V\dot{\boldsymbol{u}} + \boldsymbol{K}_V\boldsymbol{u} = -\boldsymbol{F}_w - \boldsymbol{F}_{\dot{w}} \tag{11}$$

In Eq. (11), $\boldsymbol{M}_\mathrm{V}$, $\boldsymbol{Z}_\mathrm{V}$ and $\boldsymbol{K}_\mathrm{V}$ are the mass, damping and stiffness matrices of the vehicles. $\boldsymbol{u}$, $\dot{\boldsymbol{u}}$ and $\ddot{\boldsymbol{u}}$ are the displacements, velocities and accelerations of the vehicle masses. The load vectors $\boldsymbol{F}_w$ and $\boldsymbol{F}_{\dot{w}}$ contain the primary spring and damping forces for the current motion state of the vehicle. As Eq. (11) is formulated around the static equilibrium, the spring forces F_{k1} and F_{k2} as well as the damping forces F_{c1} and F_{c2} in the vehicle's suspension systems are only activated if the vehicle bodies are in vertical motion. The Eqs. (10) and (11) are coupled through the assumption of equal displacements of the bridge (at the current position of the axles) and the unsprung vehicle masses (wheelsets).

2.3. Computation methods

The computations for this study were carried out in MATLAB [16], using the ordinary differential equation (ODE) solver *ode113* for numerical integration. *Shampine* and *Reichelt* [17] give a detailed description of the solver that is based on the *Adams-Bashforth-Moulton* method. The following computations consider the first three mode shapes of the bridge.

2.3.1. Solution for the MLM

In order to solve the EOM for the MLM, Eq. (5) must be written in a form acceptable to the chosen solver. In a first step, multiplying Eq. (5) with the inverse mass matrix and consideration of Eq. (6) leads to the explicit form:

$$\ddot{\boldsymbol{q}} = \boldsymbol{M}^{-1}\left[\sum_{i=1}^{m} F_i\Gamma_i(x_i)\phi(x_i) - \boldsymbol{Z}\dot{\boldsymbol{q}} - \boldsymbol{K}\boldsymbol{q}\right] \tag{12}$$

In a second step, Eq. (12) is transformed into a first order ODE system by substituting $\dot{\boldsymbol{q}}$ and $\boldsymbol{q}$ with new variables. *Shampine et al.* describe this transformation in detail in [18]. Finally, the resulting first order ODE system is solved with *ode113*.

2.3.2. Solution for the DIM

The vehicle-bridge interaction effects lead to the EOM from Eq. (10) for the bridge subsystem. The generalized accelerations $\ddot{\boldsymbol{q}}$ as variables to be determined in Eq. (10) are simultaneously part of the load terms on the right hand side of the equation. This algebraic loop is eliminated by excluding the terms multiplied with $\ddot{\boldsymbol{q}}$ in Eq. (10) from the load vector and writing them as part of a modified mass matrix $\boldsymbol{M}_{mod}$ [14]:

$$\boldsymbol{M}_{mod} \equiv \boldsymbol{M} + \sum_{i=1}^{m} m_{w,i}\Gamma(x_i)\phi(x_i)\phi^T(x_i) \tag{13}$$

The modified load vector $\boldsymbol{P}_{mod}$ follows as [14]:

$$\boldsymbol{P}_{mod} \equiv \sum_{i=1}^{m}\{F_i - F_{k1,i}(t) - F_{c1,i}(t) - m_{w,i}\left[2v\phi_{,x}(x_i)\dot{\boldsymbol{q}} + v2\phi_{,xx}(x_i)\boldsymbol{q}\right]\}\Gamma_i(x_i)\phi(x_i) \tag{14}$$

Making use of Eqs. (13) and (14), the EOM for the bridge subsystem can be written as:

$$\boldsymbol{M}_{mod}\ddot{\boldsymbol{q}} + \boldsymbol{Z}\dot{\boldsymbol{q}} + \boldsymbol{K}\boldsymbol{q} = \boldsymbol{P}_{mod} \tag{15}$$

In order to solve the EOM for the vehicle and the bridge subsystems simultaneously with *ode113*, Eqs. (11) and (15) are assembled in a global equation system of the form:

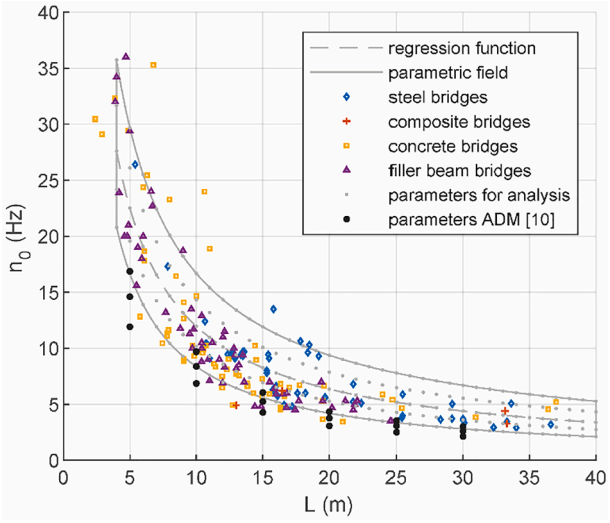

Fig. 8. Parametric field of spans L (m) and first natural frequencies n_0 (Hz).

$$\begin{bmatrix} \boldsymbol{M}_{mod} & \varnothing \\ \varnothing & \boldsymbol{M}_V \end{bmatrix} \begin{bmatrix} \ddot{\boldsymbol{q}} \\ \ddot{\boldsymbol{u}} \end{bmatrix} + \begin{bmatrix} \boldsymbol{Z} & \varnothing \\ \varnothing & \boldsymbol{Z}_V \end{bmatrix} \begin{bmatrix} \dot{\boldsymbol{q}} \\ \dot{\boldsymbol{u}} \end{bmatrix} + \begin{bmatrix} \boldsymbol{K} & \varnothing \\ \varnothing & \boldsymbol{K}_V \end{bmatrix} \begin{bmatrix} \boldsymbol{q} \\ \boldsymbol{u} \end{bmatrix} = \begin{bmatrix} \boldsymbol{P}_{mod} \\ -\boldsymbol{F}_w - \boldsymbol{F}_{\dot{w}} \end{bmatrix} \tag{16}$$

The interaction between the bridge and the vehicle subsystems is embedded in Eq. (16) through the vector $\boldsymbol{P}_{mod}$ that is dependent on the primary spring and damper forces $F_{k1,i}$ and $F_{c1,i}$ and therefore on the vehicle's displacements $\boldsymbol{u}$ and velocities $\dot{\boldsymbol{u}}$. Furthermore, the load terms of the vehicle $\boldsymbol{F}_w$ and $\boldsymbol{F}_{\dot{w}}$ are dependent on the motion of the wheelsets, which is expressed by the generalized displacements $\boldsymbol{q}$ and velocities $\dot{\boldsymbol{q}}$ of the bridge. Multiplication with the inverse global mass matrix of Eq. (16) leads to the explicit form

$$\begin{bmatrix} \ddot{\boldsymbol{q}} \\ \ddot{\boldsymbol{u}} \end{bmatrix} = \begin{bmatrix} \boldsymbol{M}_{mod} & \varnothing \\ \varnothing & \boldsymbol{M}_V \end{bmatrix}^{-1} \left(\begin{bmatrix} \boldsymbol{P}_{mod} \\ -\boldsymbol{F}_w - \boldsymbol{F}_{\dot{w}} \end{bmatrix} - \begin{bmatrix} \boldsymbol{Z} & \varnothing \\ \varnothing & \boldsymbol{Z}_V \end{bmatrix} \begin{bmatrix} \dot{\boldsymbol{q}} \\ \dot{\boldsymbol{u}} \end{bmatrix} - \begin{bmatrix} \boldsymbol{K} & \varnothing \\ \varnothing & \boldsymbol{K}_V \end{bmatrix} \begin{bmatrix} \boldsymbol{q} \\ \boldsymbol{u} \end{bmatrix} \right) \tag{17}$$

that is subsequently transformed into a first order equation system as described in the previous Section 2.3.1 and finally solved by using *ode113*. The time dependent parts of Eq. (17) – $\boldsymbol{M}_{mod}$, $\boldsymbol{P}_{mod}$, $\boldsymbol{F}_w$ and $\boldsymbol{F}_{\dot{w}}$ – are formulated as functions of time in the software, so that they are automatically recalculated for every time step of the solver.

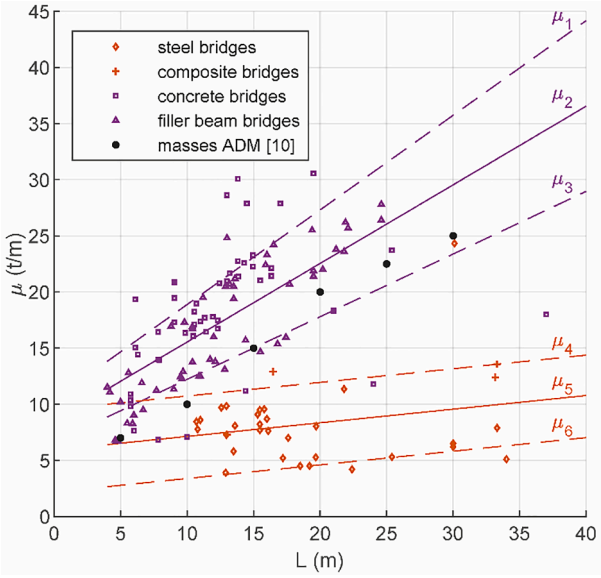

Fig. 9. Bridge masses μ in (t/m).

3. Parametric analysis

3.1. Bridge parameters

The parametric analysis performed for this paper aims to represent realistic bridge structures. As the dynamic behaviour of existing structures differs due to the wide range of bridge types, the analysis is restricted to simply supported single-track bridges with a ballast layer and a span not exceeding 40 m. The authors collected the characteristics of 210 existing bridges complying with these requirements into a database. As the authors are not aware of any pre-stressed concrete bridges at high-speed railway tracks, in this paper the expression "concrete bridges" refers to reinforced concrete bridges. The following sources were used:

- Austrian Federal Railways (OEBB): 56 concrete bridges, 10 filler beam bridges, 15 steel bridges and three composite bridges located in Austria.
- Frýba [1]: 19 concrete bridges and 17 steel bridges.
- ERRI D214/RP 3 [19]: five concrete bridges, 19 filler beam bridges, 20 steel bridges and three composite bridges located in France, Germany and Spain.
- ERRI D214/RP 8 [20]: 14 filler beam bridges and four steel bridges located in France and Spain.
- Rauert et al. [21]: 25 filler beam bridges located in Germany.

This database is used for calibrating the input parameters for the parametric analysis performed for this paper. In the following sections, the parameters applied for developing the ADM in [10] are discussed and compared to the chosen input parameters of this study.

3.1.1. Parametric field of spans and natural frequencies

The spans L in (m) and the first natural frequencies n_0 in (Hz) of the 210 existing bridges from the database are illustrated in Fig. 8. According to [1], the power regression function in the format $n_0 = aL^b$ proves best for describing the correlation between spans and first natural frequencies of railway bridges. The dashed grey line in Fig. 8 shows the proper function

$n_{0,fit} = 97.76L^{-0.9124}$ for the 210 considered bridges. The functions for the upper bound (UB)

$n_{0,UB} = 113.1L^{-0.8312}$ and the lower bound (LB) $n_{0,LB} = 82.43L^{-0.9937}$ for the parametric field are specified as 95% confidence intervals (continuous grey lines in Fig. 8) of the function $n_{0,\text{fit}}$.

The combinations of the parameters span and first natural frequency that were chosen for the analysis are depicted as grey points in Fig. 8. At each integer value of the span between four and 40 m, the values of $n_{0,\text{fit}}$, $n_{0,\text{UB}}$, $n_{0,\text{LB}}$ and two equidistant values between $n_{0,\text{fit}}$ and $n_{0,\text{UB}}$ respectively $n_{0,\text{fit}}$ and $n_{0,\text{LB}}$ are specified. In comparison to the 185 L-n_0-combinations in the present study, only 18 combinations were used in the development of the ADM in [10]. These 18 combinations (black points in Fig. 8) do not represent the existing bridges sufficiently and are split into only six span lengths of 5, 10, 15, 20, 25 and 30 m. A previous parametric study carried out by the authors [9] with a finer grid of one metre span intervals yielded VBI effects that could not have been captured within the five metre intervals defined in [10].

Preliminary investigations have shown that a categorisation into concrete and filler beam (CFB) bridges on the one hand and steel and composite (SC) bridges on the other hand leads to almost congruent parametric fields in the n_0-L-diagram. Therefore, the parametric field in Fig. 8 is specified for all considered bridge structures.

3.1.2. Bridge masses and bending stiffness

For the parametric analysis, the spans L and the first natural frequencies n_0 of the bridge structures are defined as described in the previous section. Regarding Eq. (18), which describes the first natural frequency of a simply supported Bernoulli-Euler beam [1], the mass per unit length μ or the bending stiffness EJ has to be known in order to

Table 1
Parameters for the linear regression functions μ_1 to μ_6 corresponding to Eq. (19).

	μ_1	μ_2	μ_3	μ_4	μ_5	μ_6
k	0.843	0.7002	0.5584	0.1214	0.1214	0.1214
d	10.45	8.539	6.627	9.5174	5.918	2.1691

Table 2
Values of damping to be assumed for design purposes [4].

Bridge type	ζ Lower limit of percentage of critical damping (%)	
	Span L $< 20\ m$	Span L $\geq 20\ m$
Steel and composite	$\zeta = 0.5 + 0.125(20 - L)$	$\zeta = 0.5$
Filler beam and reinforced concrete	$\zeta = 1.5 + 0.07(20 - L)$	$\zeta = 1.5$

allow the determination of the other missing parameter.

$$n_0 = \frac{\pi}{2L^2}\sqrt{\frac{EJ}{\mu}} \tag{18}$$

Especially for concrete structures, the bending stiffness of existing bridges is difficult to assess due to the time-dependent development of the Young's modulus E, the influence of cracking and a lack of measured data. Conversely, the bridge masses can usually be estimated with acceptable accuracy by analysing the cross section of the bridge. For 152 bridges of the database, the mass per unit length μ is known and depicted as a function of the span in Fig. 9.

In order to obtain realistic bridge masses for the parametric analysis, it is advisable to categorise the bridges into CFB structures on the one hand (purple markers in Fig. 9) and SC structures on the other hand (orange markers in Fig. 9). The continuous lines in Fig. 9 are the linear regression functions μ_2 for CFB and μ_5 for SC bridges. For the CFB bridges, the 95% confidence intervals of the linear regression function are additionally taken into account in the analysis as upper bound (UB) function μ_1 and lower bound (LB) function μ_3 (dashed purple lines in Fig. 9). Due to the rather small number of SC bridges, the 95% confidence interval would lead to a LB function with a negative gradient, which is not mechanically reasonable. Therefore, the UB μ_4 and LB μ_6 for SC bridges are set as linear functions (dashed purple lines in Fig. 9) with the same gradient as the regression function, but shifted so that only two mass values of the existing SC bridges exceed the chosen boundaries in each direction. The obtained mass functions μ_1 up to μ_6 are numbered from high to low masses and defined by Eq. (19) and the parameters in Table 1.

$$\mu(L) = kL + d;\ \mu \ \text{ in } \ (\text{t/m}) \ \text{ and } \ L \ \text{ in } \ (\text{m}) \tag{19}$$

The bridge masses used in [10] to derive the ADM are depicted in Fig. 9 as black points. A fixed mass value was allocated for each considered span. Although these mass values are close to the LB function μ_3 for CFB bridges, they are not representing existing SC bridges at all. Furthermore, VBI effects are decreasing at higher bridge masses for a fixed frequency ratio between the bridge and the vehicle [5–7], which is why UB values for the bridge masses should be chosen in order to obtain conservative results of additional damping values.

3.1.3. Damping

Unless the real structural damping of a bridge is determined experimentally, the damping for dynamic analyses is prescribed in the Eurocode [4] depending on the bridge type and the span as shown in Table 2.

Inter alia, VBI effects depend on the structural damping [5,6]. This means that if it is attempted to take into account VBI effects by considering additional damping in MLM analyses, the proper value of the additional damping can be affected by the base value of structural damping. In [10], the fixed values of 0.5, 1.0 and 2.0% were used as structural damping for all considered spans (see black points in Fig. 10) to calibrate the ADM. This choice yields several situations that are not matching the base values given in Eurocode [4] as the damping is too low for short span bridges and too high especially for longer span SC bridges.

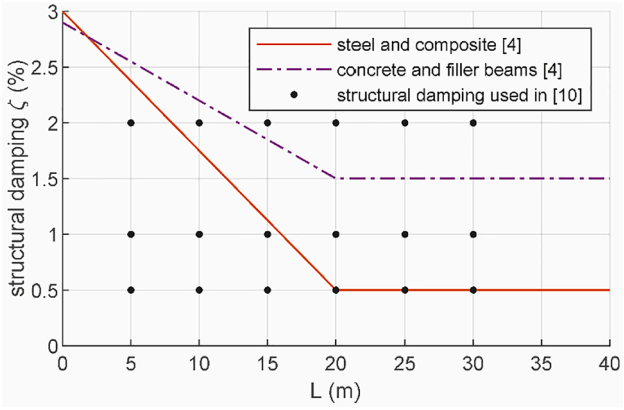

Fig. 10. Structural damping ζ (%).

For this study, the base values given in the Eurocode (see Table 2 and Fig. 10) are used as structural damping both for MLM and DIM analyses. As a further consequence, the additional damping describing the differences between these two models is in line with the commonly used base values.

3.1.4. Concluding remarks for the chosen bridge parameters

The parametric field of spans and natural frequencies is representing existing simply supported, single-track bridges with ballast layer and spans between four and 40 m (see Fig. 8). Concrete and filler beam bridges are represented in the parametric analysis by the mass functions μ_1 to μ_3, steel and composite bridges by the mass functions μ_4 to μ_6 (Fig. 9). The damping is set depending on the bridge type and the span according to the Eurocode (Fig. 10).

3.2. Vehicle parameters

In [10], the ADM was calibrated for the train transit of the ICE-2 and an Eurostar configuration over the parameterised bridges. Additionally to these two trains, the German ICE-4 and the Austrian Railjet were investigated for this study. The detailed train parameters of all examined trains are specified in detail in Table A1.

A major concern in the evaluation of additional damping is the conformity of static loads for the MLM and the DIM. Concerning the DIM, the bridge loads result from the real vehicle masses (consisting of dead weight and live loads) and the motion during a train transit. Conversely, the single vertical loads for the MLM defined in standards and regulations can contain additional safety factors that are often not commonly comprehensible. In the latter case, a comparison with an interaction model with real vehicle masses would lead to additional damping values that are not only restricted to the mechanical VBI effect, but contain a certain amount of artificial amplification. For all analyses carried out in this study, several single loads for the MLM are based on the real vehicle masses, so that only the sole VBI effect is considered in the evaluation of the additional damping.

3.2.1. ICE-2

The ICE-2 is a conventional train with two bogies per car body. It consists of 12 passenger cars (PC) and one locomotive (Loc) at both ends of the train (see Fig. 11). The train parameters and the axle loads are documented in [10].

3.2.2. Eurostar

The Eurostar is a train with Jacobs bogies. The investigated configuration consists of two flipped sets of nine PCs each, which are operated by a total of two locomotives, one at each end of the train (see Fig. 12).

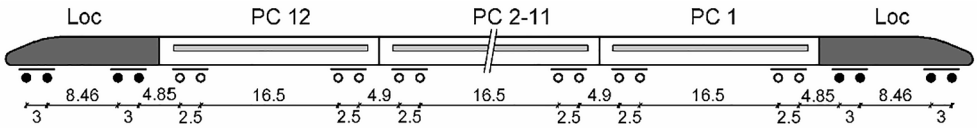

Fig. 11. ICE-2 configuration and axle distances in (m).

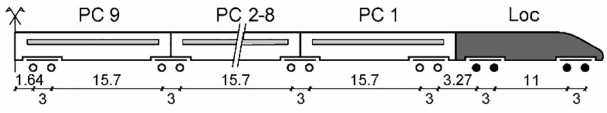

Fig. 12. Eurostar configuration and axle distances in (m).

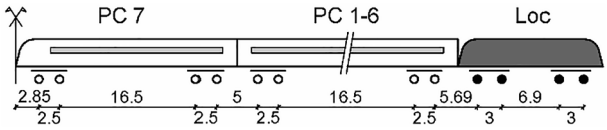

Fig. 13. Railjet configuration and axle distances in (m).

The train parameters are documented in [10] and additional geometrical information is taken from [22] to set up the train model in detail. The locomotives are assumed to have no vertical connection to the passenger cars in the train model. The PCs numbers 1 and 9 have one conventional bogie on one side and share a Jacobs bogie with the adjacent cars on the other side.

The axle loads for the Eurostar are uniformly assumed to 170 kN in [10]. In contrast, the multiplication of the real vehicle masses (dead weight and live loads) with the gravitational acceleration of 9.81 m/s^2 leads to axle loads of 153.8 kN (≈10% less) for the locomotive and 143.3 kN (≈16% less) for the PCs. Therefore, the determined additional damping for the Eurostar in [10] not only represents the VBI effects, but also includes an imbalance of the static axle loads.

3.2.3. Railjet

The Railjet is a high-speed train operating in Austria and in some neighbouring countries. The considered configuration consists of two sets of seven PCs each, which are driven by two locomotives, one at each end of the train (see Fig. 13). The train parameters are documented in [8].

3.2.4. ICE-4

The considered configuration of the German high-speed train ICE-4 consists of six powered and six unpowered PCs. The powered cars are marked through filled black wheelsets in Fig. 14. The bogies for powered and unpowered cars differ in their masses, suspension parameters and wheelset distances. The detailed train parameters are documented in [23].

3.3. Scope of the parametric analysis

In total, the specified L-n_0 parametric field and the six mass functions lead to 1110 parameterised bridges, which are analysed for the four train types and both vehicle models, the MLM and the DIM. In accordance with [10], we defined a speed range from 160 to 350 km/h for the computations. In order to capture all possible maximum responses of the bridge accurately, we performed the MLM analyses using 1 km/h steps throughout the defined speed range. In order to limit the computational expenses of the DIM analyses, we chose a step size of 5 km/h and refined the computation in the area of the maximum response speed v_{max} for the MLM. Therefore, we additionally used 1 km/h steps in the interval v_{max}-20 km/h to v_{max} + 5 km/h. Finally, we controlled visually, if the peak response for the DIM was captured within the 1 km/h interval accurately and added minor refinements of the DIM speed steps where necessary.

4. Evaluation and results

In the following evaluations, we investigate the maximum vertical bridge deck acceleration at midspan. The limitation of this value is essential to avoid ballast destabilisation, risk of derailment, deterioration of passenger comfort and a raise in maintenance costs [6]. Therefore, the maximum vertical accelerations within a certain speed range are of great interest for design and verification purposes.

The determination of the additional damping within this study follows three steps. It is shown for a selected bridge in Fig. 15.

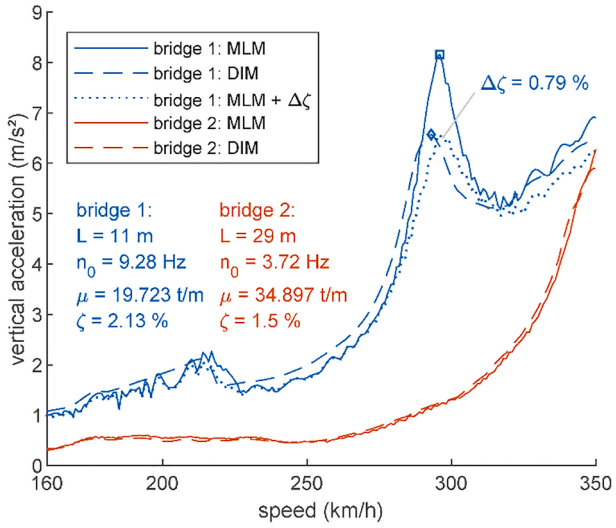

Fig. 15. Maximum vertical accelerations of two selected bridges and varying vehicle models of the ICE-2.

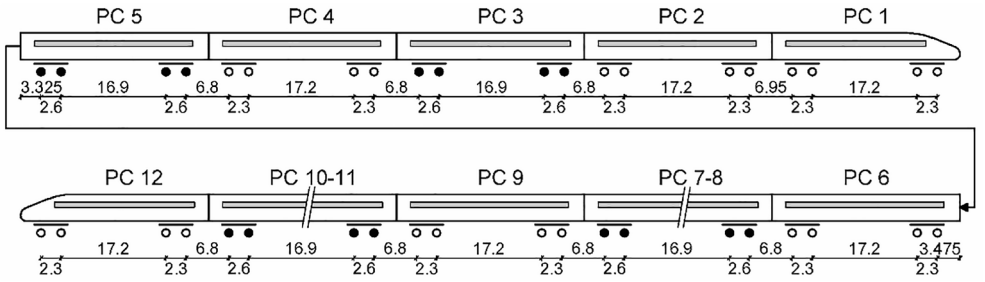

Fig. 14. ICE-4 configuration and axle distances in (m).

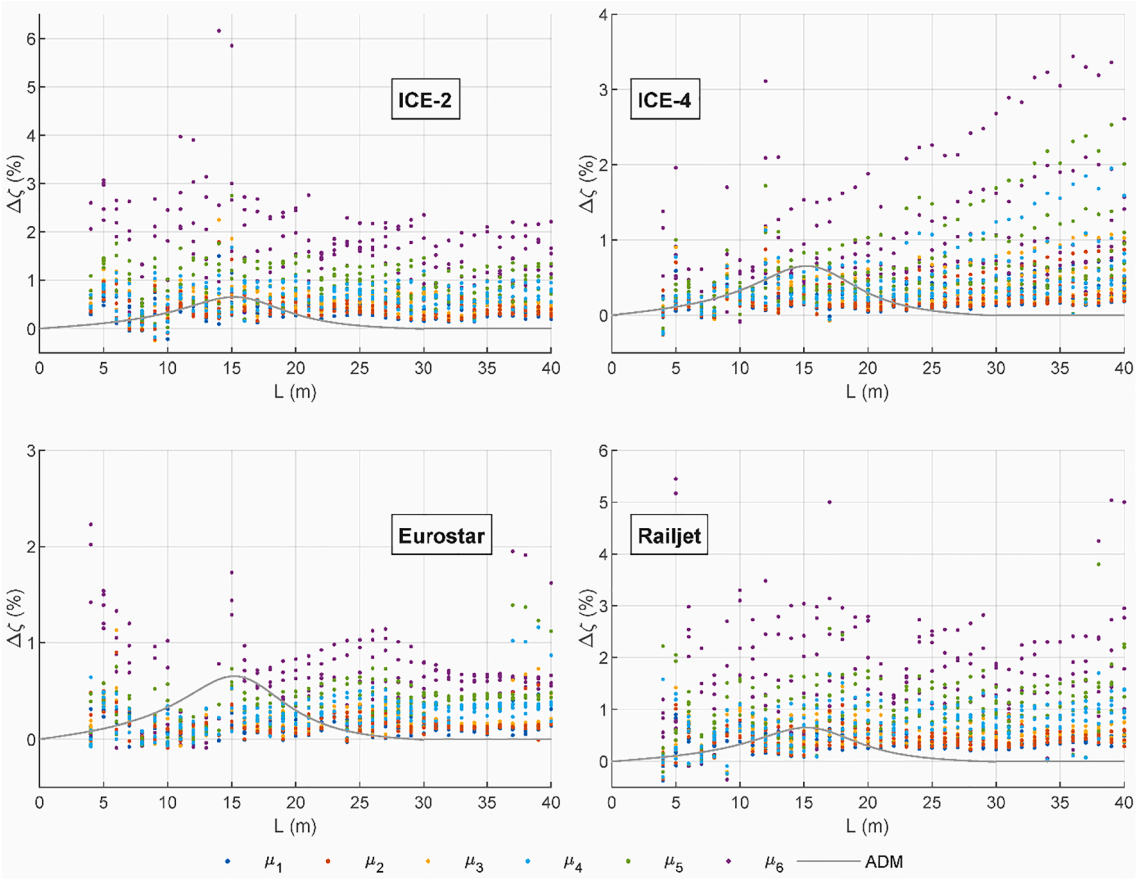

Fig. 16. Comparison between computed results and the ADM for each train.

- Step 1: The maximum vertical accelerations for the MLM and the DIM are plotted as a function of the train speeds.
- Step 2: The maximum peak value of the MLM and the associated peak value of the DIM are identified (see marks for bridge 1 in Fig. 15). We considered only peaks that are also local maxima. This means that maximum accelerations at 350 km/h (see bridge 2 in Fig. 15) were excluded from the further investigations, as the additional damping can be reasonably evaluated only by comparing real peak values for the MLM and the DIM. In some situations, no reasonable peak values could be found (see bridge 2 in Fig. 15).
- Step 3: The structural damping of the MLM is modified iteratively in steps of 0.01%, until the peak value of this adapted model equals the peak value of the DIM with an accuracy of 0.1%. The required additional damping (denoted as $\Delta\zeta$) is the subject for further evaluations.

4.1. Additional damping: Computed results vs. Eurocode

In Fig. 16, the computed values of $\Delta\zeta$ are depicted for the four considered train types with respect to the span L. The results illustrate that the additional damping as defined in the Eurocode (grey line in Fig. 16) yields non-conservative values for a large number of bridges and each of the regarded train types. Moreover, a negative additional damping would be necessary for some short span bridges (approx. L < 10 m) in order to equal the MLM results to those of the DIM. The rather volatile values of the additional damping for short and medium span bridges ($L < 20$ m) make a definition of a useful and conservative correlation between $\Delta\zeta$ and L impossible for these bridges. On the other hand, the additional damping for bridges with larger spans (approx. $L >$ 25 m) takes on rather stable values beyond zero. For these bridges, the ADM is unnecessarily conservative. Therefore, the limitation of the ADM to bridges with $L < 30$ m in the Eurocode is not reasonable.

Additionally, the results in Fig. 16 verify the tendency of increasing additional damping values for lower bridge masses (at a fixed frequency ratio between the bridge and the vehicle). However, this statement cannot be generalized as even the lightest mass function μ_6 yields negative additional damping values for single bridges (see ICE-4, Eurostar and Railjet for spans $L \approx 10$ m in Fig. 16).

4.2. Additional damping as a function of bridge frequencies

Arvidsson et al. [11] recommend to consider the additional damping as a function of bridge frequencies, as the ratio between bridge and vehicle frequencies is identified as a major factor in the VBI [6,11]. This approach allows the definition of lower bound functions for the additional damping, for each train separately and for the considered mass functions of the bridge.

4.2.1. Definition of a lower bound function

The computed additional damping for the ICE-2 and the mass μ_3 is depicted in Fig. 17 as a function of the natural bridge frequency. In order to define a lower bound (LB) function, the whole range of possible bridge frequencies is divided into intervals, which are containing approximately 10 computed values of $\Delta\zeta$ each. Therefore, the interval width of 0.5 Hz is set between 2 and 8 Hz, the further boundaries are set at 9, 10, 11, 13, 16 and 21 Hz. The minimum values of $\Delta\zeta$ in each interval (yellow points in Fig. 17) serve as data points to fit a LB function using the linear least squares method. In order to represent these data points appropriately without overfitting, a cubic polynomial in the format

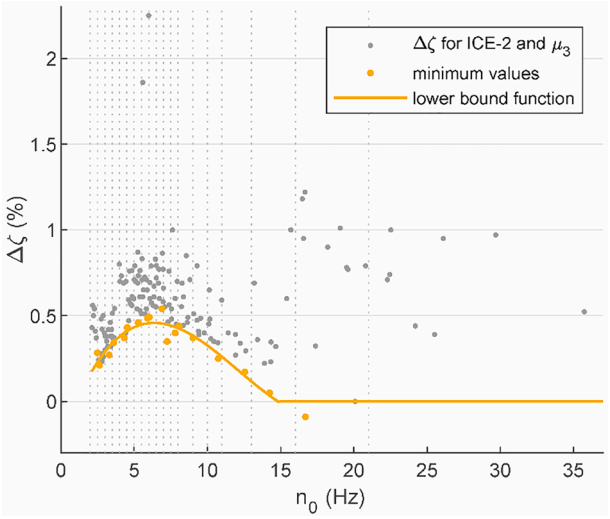

Fig. 17. Lower bound of additional damping Δζ; ICE-2 and μ_3.

$$\Delta\zeta(n_0) = an_0^3 + bn_0^2 + cn_0 + d \tag{20}$$

is chosen as fit function. As negative values of $\Delta\zeta$ occur for each considered train, the lower bound of $\Delta\zeta$ is set to zero from the first intersection of the fitted polynomial with the abscissa. Although the additional damping for bridges with high natural frequencies of 21 Hz and more seems to increase, this effect is not taken into account due to the small number of results for such bridges.

For the fitted LB function in Fig. 17, the coefficient of determination R^2 with respect to the yellow data points is 0.931. The minimum residual of −0.098% occurs for the data point at 7.24 Hz, which means that the difference of additional damping between this data point and the LB function is −0.098%. The maximum residual of 0.086% occurs for the data point at 6.89 Hz.

4.2.2. Lower bounds of additional damping

The method described in the previous section is used for deriving LB functions for all regarded trains and mass functions (see Fig. 18). These LB functions are applicable between 2.1 Hz and their first intersection with the abscissa. The numerical values for the derived LB functions, their coefficients of determination R^2 and their minimum and maximum residuals are given in Appendix B, Tables B1-B4.

As shown in Fig. 18, $\Delta\zeta$ takes the highest values for the ICE-2 in the area of equal bridge and bogie frequencies ($n_p = 5.84$ Hz, see Eq. (1)). Thus, the ratio between bridge and bogie frequency seems to be the governing parameter in the VBI for this train. The similar effect can be observed for the Eurostar ($n_p = 3.18$ Hz) at a lower extent. For the ICE-4, the bogie frequencies for powered/unpowered cars ($n_p = 4.78$ Hz|16.52 Hz) are not consistent over the train length. For this reason, their influence on the VBI does not appear in Fig. 18. For the Railjet ($n_p = 5.53$ Hz), the additional damping stays rather constant in a broad range of bridge frequencies. The ratio between bridge and bogie frequencies does not seem to be the governing parameter for VBI effects of this train.

The orange lines representing SC bridges and the purple lines representing CFB bridges in Fig. 18 show that the VBI is generally higher for lower bridge masses. The higher additional damping for SC bridges is additionally influenced by lower structural damping values compared to CFB bridges.

Generally, the VBI effects and thus the proper additional damping values are different for each of the considered train types, the bridge types and the bridge masses. Furthermore, every attempt to describe these effects with one simplified definition for the additional damping that is universally valid for all train and bridge types either leads to conservative $\Delta\zeta$-values close to zero or to significantly non-conservative values for some train-bridge combinations. In the first case, the ADM is hardly beneficial and in the latter case, the ADM does not meet the requirements for standardisation or directives regarding the dynamic analysis of train transits. Therefore, further simplifications in terms of one resulting $\Delta\zeta$-function for certain train or bridge types or the application of the computed results for other than the investigated train types

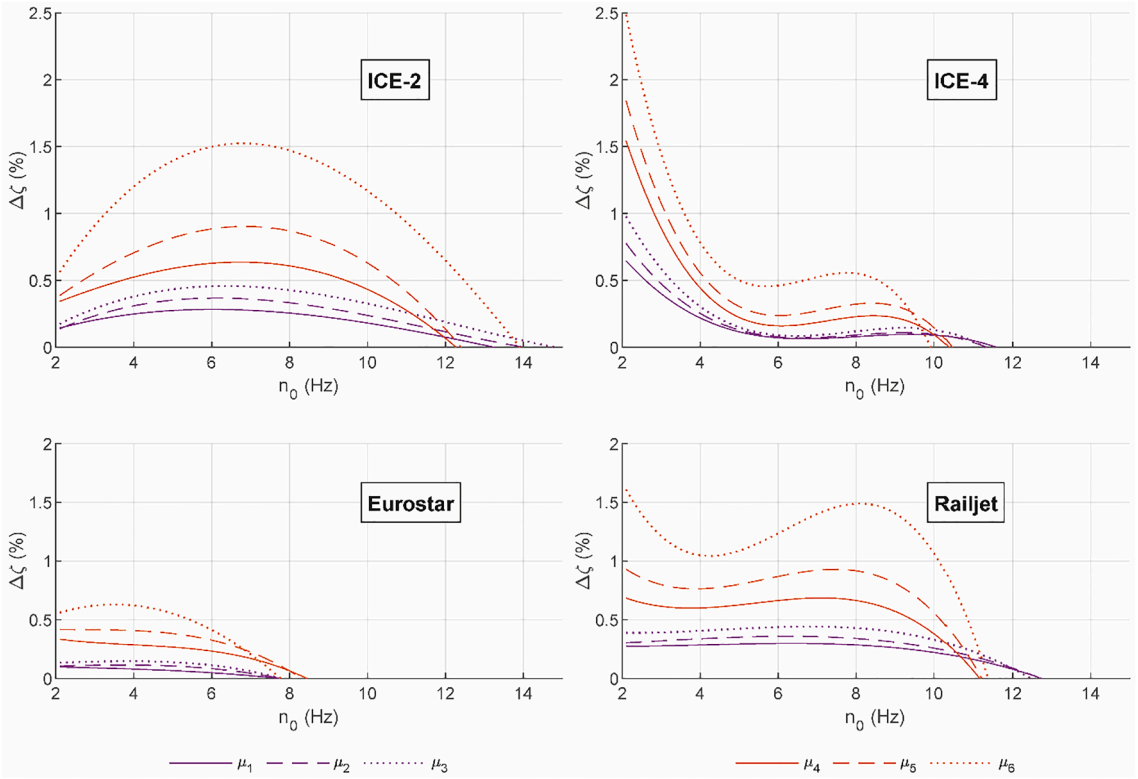

Fig. 18. Lower bounds of additional damping for each train.

Table 3
Parameters of the selected bridges.

Bridge	L (m)	n_0 (Hz)	μ (t/m)	EJ (Nm^2)	ζ (%)
B1	15	8.26	19.042	2.667e10	1.85
B2	30	3.60	29.545	1.256e11	1.50
B3	15	8.26	7.739	1.084e10	1.13
B4	30	3.60	9.560	4.064e10	0.50

are not recommended.

4.3. Application of the results

In the dynamic analysis of a simply supported railway bridge, the span L, the mass per unit length μ, the bending stiffness EJ and the first natural frequency n_0 of the bridge are usually known from construction plans or from experiments. In the few cases where μ of the regarded bridge is outside the UB and LB functions (μ_1 and μ_3 for CFB bridges; μ_4 and μ_6 for SC bridges), $\Delta\zeta$ can be taken directly from Fig. 18 for the nearest related UB or LB function depending on the span length and the regarded train. For values of μ inside the UB and LB functions, $\Delta\zeta$ can be taken on the safe side for the next highest mass function μ_1 or μ_2 for CFB bridges, respectively, μ_4 or μ_5 for SC bridges from Fig. 18. Alternatively, $\Delta\zeta$ can be determined more accurately by linear interpolation between the values for the adjacent mass functions.

As stated in the previous section, this method should only be applied for the investigated train types.

4.4. Comparison of different additional damping approaches for four selected bridges

In this section, the computed results and the lower bound functions of this study are compared with the ADM and the EADA for four selected bridges with two different spans. For the selected shorter span of $L = 15$ m, the ADM yields almost its maximum additional damping values. The chosen longer span of $L = 30$ m enables investigations at the application boundary of the ADM. The bridges B1 and B2 represent CFB bridges in line with the mass function μ_2 (see Section 3.1.2). The bridges B3 and B4 represent SC bridges in line with the mass function μ_5. The detailed parameters of the selected bridges are collected in Table 3.

In Fig. 19, the total damping $\zeta_{tot} = \zeta + \Delta\zeta$ is depicted as sum of the structural damping ζ due to Table 2 (grey bars) and the additional damping $\Delta\zeta$ for different approaches. Herein, $\Delta\zeta_{VBI}$ (blue bars) is the computed amount of additional damping to equal the maximum accelerations of the MLM to those of the DIM, $\Delta\zeta_{LB}$ (orange bars) results from applying the lower bound functions from Section 4.2.2 of this study, $\Delta\zeta_{ADM}$ (yellow bars) represents the ADM due to the Eurocode and $\Delta\zeta_{EADA}$ (purple bars) shows the EADA results due to Eq. (3). The numerical values for the different additional damping approaches are collected in Table 4. As the vehicle model of the Eurostar is not consistent with the initial assumptions of the EADA, $\Delta\zeta_{EADA}$ is not determined for this train. The evaluation of $\Delta\zeta_{EADA}$ for the ICE-4 is performed for the vehicle parameters of the unpowered PCs.

Regarding the results for the shorter span CFB bridge B1 from Fig. 19, the ADM is non-conservative for each train type. For the shorter span SC bridge B3, the ADM yields useful conservative results

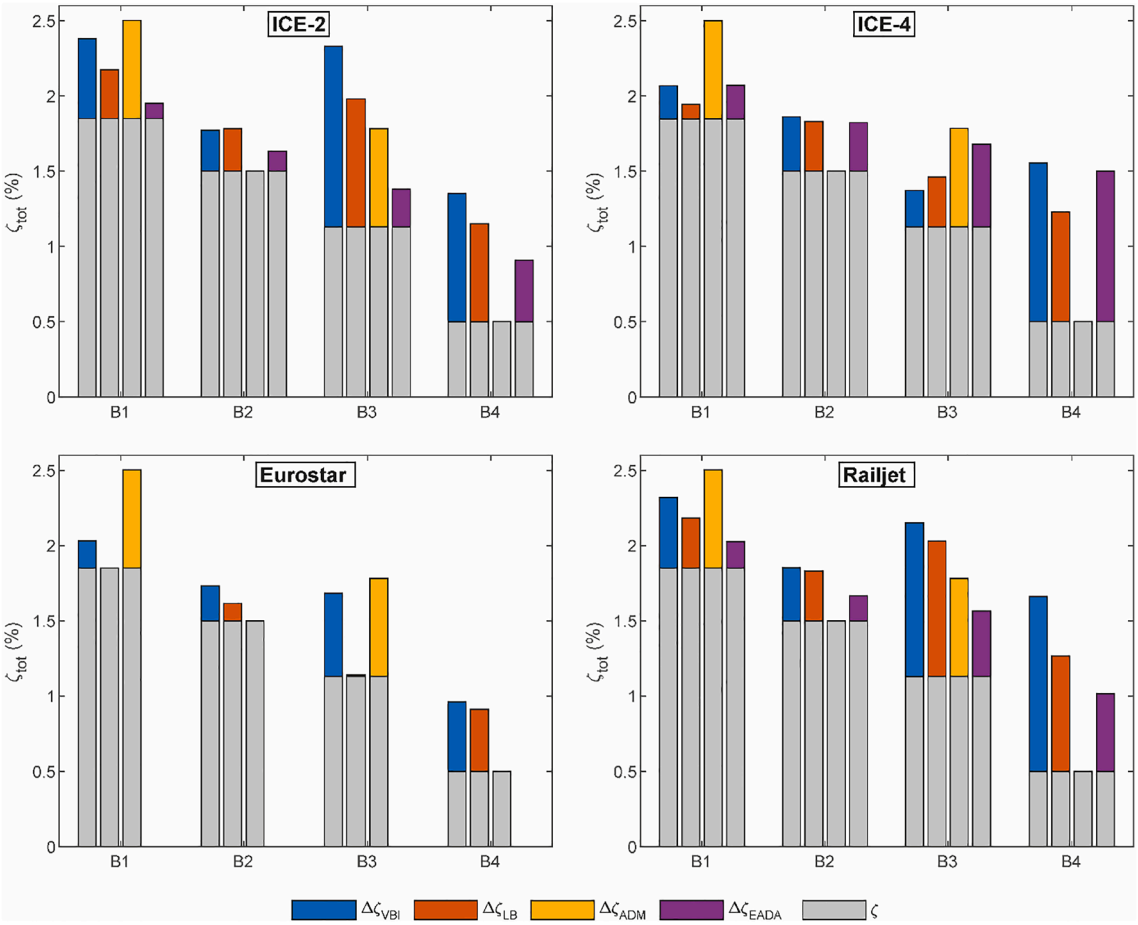

Fig. 19. Total damping for different approaches and four selected bridges.

Table 4
Additional damping $\Delta\zeta$ (%) for different approaches.

	ICE-2				Eurostar				Railjet				ICE-4			
	B1	B2	B3	B4	B1	B2	B3	B4	B1	B2	B3	B4	B1	B2	B3	B4
$\Delta\zeta_{VBI}$	0.53	0.27	1.20	0.85	0.18	0.23	0.55	0.46	0.47	0.35	1.02	1.16	0.22	0.36	0.24	1.06
$\Delta\zeta_{LB}$	0.32	0.28	0.85	0.65	0	0.12	0.01	0.41	0.33	0.33	0.90	0.77	0.10	0.33	0.33	0.73
$\Delta\zeta_{ADM}$	0.65	0	0.65	0	0.65	0	0.65	0	0.65	0	0.65	0	0.65	0	0.65	0
$\Delta\zeta_{EADA}$	0.10	0.13	0.25	0.41	–	–	–	–	0.18	0.17	0.44	0.51	0.22	0.32	0.55	1.00

for the ICE-2 and the Railjet, slightly non-conservative values for the Eurostar and clearly non-conservative values for the ICE-4. For the longer span bridges B2 and B4 the ADM does not provide any additional damping, which is unnecessarily conservative especially for the SC bridge B4.

Due to Fig. 19, the lower bound functions presented in this study prove to be a useful approximation of the additional damping. Only for the ICE-2 at B2 and the ICE-4 at B3, the method slightly over-estimates the additional damping. The fundamental frequency of the bridge B1 is outside the application boundaries for the Eurostar, so that $\Delta\zeta_{LB} = 0$ in this situation.

For the ICE-4, the EADA estimates the additional damping almost perfectly for the bridges B1, B2 and B4. However, it slightly over-estimates the additional damping for B3 for this train. For the ICE-2 and the Railjet, the EADA consistently yields conservative additional damping values.

5. Conclusions

Proper additional damping has been determined for a parametric field of 185 simply supported single-track bridges with a ballast layer, six different masses for each bridge and the four high-speed trains ICE-2, Eurostar, Railjet and ICE-4. An iterative process was used until the peak vertical accelerations at midspan calculated with the MLM (Moving Load Model) were adjusted to the corresponding values calculated with the DIM (Detailed Interaction Model). The importance of VBI (vehicle-bridge interaction) corresponds directly to the amount of necessary additional damping. The following conclusions can be drawn from this study:

1. Additional damping has a significantly clearer correlation to the natural bridge frequency than to the span length. Therefore, lower bounds for the additional damping are defined as functions of the natural bridge frequencies, but also depending on the bridge mass and the train type.
2. The influence of the ratio between the bridge and vehicle mass on the VBI is clearly visible in the six selected mass functions. The additional damping increases with lower bridge masses. Therefore, it is useful to distinguish heavier CFB (concrete and filler beam) bridges from lighter SC (steel and composite) bridges. This also allows for the consideration of the commonly used values of structural damping according to the Eurocode in the parametric study.
3. Additional damping differs significantly depending on the train type. Therefore, the results should only be used for the analysed train types.
4. For bridges with high natural frequencies (mostly short span bridges), additional damping is set to zero due to the wide-ranging results and due to the relatively low number of investigated structures. Additional damping is rather high for some of these bridges and negative for others. Further investigations are necessary in order to determine if it is useful to describe the VBI effects solely through additional damping for these structures as well.
5. The additional damping method (ADM) as integrated in the Eurocode is non-conservative for any of the regarded train types. Moreover, the limitation of the ADM for bridges with $L < 30$ m is not reasonable, as the computed results of the additional damping yield rather stable values beyond zero for larger span bridges (30 m $\leq L \leq$ 40 m).

Declaration of Competing Interest

The authors declare that they have no known competing financial interests or personal relationships that could have appeared to influence the work reported in this paper.

Acknowledgement

The authors acknowledge TU Wien Bibliothek for financial support through its Open Access Funding Programme.

Appendix A. . Train parameters

The detailed train parameters are described in Section 1 and depicted in Fig. 1, Fig. 2 and Fig. 3. The numerical values for the train types ICE-2, Eurostar, Railjet and ICE-4 are collected in Table A1.

Table A1
Train parameters.

Parameter	Unit	ICE-2 [10]		Eurostar [10]				Railjet [8]		ICE-4 [23]	
		Loc	PC	Loc	PC 1	PC 2-8	PC 9	Loc	PC	powered PC	unpowered PC
m_c	kg	60,768	33,930	51,500	35,860	22,525	27,122	51,500	47,316	52,896	55,279
J_c	kgm^2	1.344e6	2.115e6	1.05e6	1.658e6	0.81e6	1.254e6	8.82e5	3.07e6	3.55e6	3.91e6
m_b	kg	5600	2373	2200	2200	2900	2900	13,220	2800	4427	2414
J_b	kgm^2	21,840	1832	1900	1900	2508	2508	27,100	1700	3090	770
m_w	kg	2003	1728	1700	1700	1900	1900	2495	1900	2322	1430
k_s	N/m	1.76e6	3e5	3.26e6	0.9e5	5.8e5	2.5e5	2.72e6	2.8e5	5e6	7.2e5
k_p	N/m	4.8e6	1.6e6	2.6e6	2.6e6	2e5	1.32e6	3.68e6	1.69e6	2e6	1.3e7
c_s	Ns/m	1.52e5	6e3	0.9e5	2e4	/	2e4	2e5	1.4e4	2e4	1e4
c_p	Ns/m	1.08e5	2e4	0.12e5	1.2e4	1.2e4	1.2e4	8e4	2e4	2e4	/
d	m	20.9	26.4	22.5	21.845	18.7	21.965	19.28	26.5	28.75	28.75
r	m	11.5	19	14	18.7	/	18.7	9.9	19	19.5	19.5
b	m	3	2.5	3	3	3	3	3	2.5	2.6	2.3
F	kN	196	112	153.8	152.1/139.4	143.3	143/111	215.6	148.4	174.2	161.4

Appendix B. . Numerical values for lower bound functions

Table B1
Parameters for LB functions ICE-2 according to Eq. (20); $\Delta\zeta$ in (%); n_0 in (Hz).

Train	Bridge mass	a	b	c	d	Upper limit (Hz)	R^2	Max. res. (%)	Min. res. (%)
ICE-2	μ_1	3.231e-4	−0.01361	0.1289	−0.07025	13.25	0.88	0.07722	−0.08517
	μ_2	6.926e-4	−0.02412	0.2177	−0.2199	14.02	0.8994	0.08938	−0.08367
	μ_3	7.282e-4	−0.02644	0.2478	−0.236	14.81	0.931	0.08573	−0.09826
	μ_4	−6.987e-4	−0.002785	0.1327	0.08258	12.27	0.7411	0.2526	−0.2034
	μ_5	−6.434e-4	−0.0126	0.264	−0.107	12.41	0.7577	0.2943	−0.3083
	μ_6	1.139e-3	−0.06146	0.6776	−0.5997	13.91	0.8498	0.306	−0.3328

Table B2
Parameters for LB functions Eurostar according to Eq. (20); $\Delta\zeta$ in (%); n_0 in (Hz).

Train	Bridge mass	a	b	c	d	Upper limit (Hz)	R^2	Max. res. (%)	Min. res. (%)
Eurostar	μ_1	−2.591e-4	0.00138	−0.00994	0.1146	7.75	0.9315	0.01474	−0.01716
	μ_2	−5.37e-4	0.001198	0.01328	0.07694	7.78	0.9327	0.02308	−0.2602
	μ_3	−0.001008	0.006074	−0.001486	0.1201	7.80	0.9488	0.02788	−0.03093
	μ_4	−0.002363	0.02815	−0.1286	0.5019	8.45	0.8649	0.06619	−0.04498
	μ_5	−0.002322	0.01912	−0.05523	0.4709	8.31	0.9497	0.08058	−0.0419
	μ_6	6.386e-5	−0.03572	0.2484	0.1952	7.77	0.8232	0.2463	−0.1986

Table B3
Parameters for LB functions Railjet according to Eq. (20); $\Delta\zeta$ in (%); n_0 in (Hz).

Train	Bridge mass	a	b	c	d	Upper limit (Hz)	R^2	Max. res. (%)	Min. res. (%)
Raljet	μ_1	−5.631e-4	0.007015	−0.02098	0.2931	12.74	0.8611	0.07455	−0.05901
	μ_2	−5.083e-4	0.004266	0.006318	0.2768	12.73	0.8679	0.1035	−0.06763
	μ_3	−0.001104	0.01497	−0.05015	0.4376	12.47	0.8698	0.1421	−0.1117
	μ_4	−0.004615	0.07522	−0.3699	1.172	11.15	0.6573	0.3317	−0.1757
	μ_5	−0.007272	0.1238	−0.6329	1.78	11.21	0.6261	0.5104	−0.2401
	μ_6	−0.01547	0.2867	−1.598	3.844	11.37	0.6874	0.4025	−0.3079

Table B4
Parameters for LB functions ICE-4 according to Eq. (20); $\Delta\zeta$ in (%); n_0 in (Hz).

Train	Bridge mass	a	b	c	d	Upper limit (Hz)	R^2	Max. res. (%)	Min. res. (%)
ICE-4	μ_1	−0.003214	0.07749	−0.6049	1.604	11.58	0.9407	0.06067	−0.05099
	μ_2	−0.004115	0.09777	−0.7529	1.964	11.32	0.9449	0.07996	−0.06977
	μ_3	−0.005526	0.1301	−0.9886	2.531	11.29	0.9443	0.1027	−0.09913
	μ_4	−0.01156	0.252	−1.783	4.283	10.37	0.8828	0.2637	−0.2303
	μ_5	−0.01389	0.3006	−2.11	5.076	10.46	0.9145	0.1934	−0.3303
	μ_6	−0.02314	0.4684	−3.087	7.118	9.92	0.9111	0.2858	−0.4821

The lower bound functions for each considered train are defined as cubic polynomials. The results are depicted in Fig. 18, their numerical values can be obtained by applying the parameters from the following Tables B1-B4 to Eq. (20). The application boundaries for the resulting polynomials are set to 2.1 Hz as lower limit and their first intersection with the abscissa as upper limit. The respective upper limits for every train and bridge mass are also given in Tables B1-B4.

References

[1] Frýba L. Dynamics of Railway Bridges. Thomas Telford; 1996.
[2] Yang Y, Yau J, Hsu L. Vibration of simple beams due to trains moving at high speeds. Eng Struct 1997;19(11):936–44.
[3] Museros P, Moliner E, Martinez-Rodrigo M. Free vibrations of simply-supported beam bridges under moving loads: maximum resonance, cancellation and resonant vertical acceleration. J Sound Vib 2013;332(2):326–45. https://doi.org/10.1016/S0141-0296(97)00001-1.
[4] EN 1991-2, Eurocode 1: Actions on structures – Part 2: Traffic loads on bridges. CEN, Brussels; 2012.
[5] Liu K, De Roeck G, Lombaert G. The effect of dynamic train-bridge interaction on the bridge response during a train passage. J Sound Vib 2009;325:240–51. https://doi.org/10.1016/j.jsv.2009.03.021.
[6] Doménech A, Museros P, Martínez-Rodrigo MD. Influence of the vehicle model on the prediction of the maximum bending response of simply-supported bridges under high-speed railway traffic. Eng Struct 2014;72:123–39. https://doi.org/10.1016/j.engstruct.2014.04.037.
[7] Doménech A, Museros P. Influence of the vehicle model on the response of high-speed railway bridges at resonance. Analysis of the additional damping method prescribed by Eurocode 1. In: Proceedings of the 8th International Conference on Structural Dynamics, EURODYN 2011; 2011. p 1273–80.
[8] Glatz B, Fink J. Einfluss der Zugmodelle auf die dynamische Antwort von 75 Stahl-, Verbund- und Stahlbetonbrücken. Stahlbau 2019;88(5):470–7. https://doi.org/10.1002/stab.201900014.
[9] Glatz B, Fink J, Bettinelli L. Triebfahrzeuge und Fahrzeug-Brücken-Interaktion in der dynamischen Berechnung von Eisenbahnbrücken. Bautechnik 2020;97(7):453–61. https://doi.org/10.1002/bate.201900113.
[10] ERRI. D214/RP 4. Train Bridge Interaction. European Rail Research Institute; 1999.
[11] Arvidsson T, Karoumi R, Pacoste C. Statistical screening of modelling alternatives in train-bridge interaction systems. Eng Struct 2014;59:693–701. https://doi.org/10.1016/j.engstruct.2013.10.008.
[12] Yau JD, Martínez-Rodrigo MD, Doménech A. An equivalent additional damping approach to assess vehicle-bridge interaction for train-induced vibration of short-span railway bridges. Eng Struct 2019;188:469–79. https://doi.org/10.1016/j.engstruct.2019.01.144.
[13] Knothe K, Stichel S. Rail Vehicle Dynamics. Basel: Springer International Publishing; 2017.
[14] Mähr TC. Theoretische und experimentelle Untersuchungen zum dynamischen Verhalten von Eisenbahnbrücken mit Schotteroberbau unter Verkehrslast. Dissertation, TU Wien; 2008.
[15] Clough RW, Penzien J. Dynamics of Stuctures. 3rd ed. Berkeley: Computers & Structures, Inc.; 2003.

[16] MATLAB. Version 9.5.0.944444 (R2018b). Natick, Massachusetts: The MathWorks Inc.; 2018.
[17] Shampine LF, Reichelt MW. The MATLAB ODE Suite. SIAM J Sci Comput 1997;18 (1):1–22. https://doi.org/10.1137/S1064827594276424.
[18] Shampine LF, Gladwell I, Thompson S. Solving ODEs with MATLAB. Cambridge: Cambridge University Press; 2003.
[19] ERRI D214/RP 3. Recommendations for calculating damping in rail bridge decks. European Rail Research Institute; 1999.
[20] ERRI D214/RP 8. Confirmation of values against experimental data. Part B: Comparison of calculations and measurements using simplified models of rail bridges. European Rail Research Institute; 1999.
[21] Rauert T, Bigelow H, Hoffmeister B, Feldmann M, Patz R, Lippert P. Zum Einfluss baulicher Randbedingungen auf das dynamische Verhalten von WIB-Eisenbahnbrücken. Teil 1: Einführung und Messuntersuchungen an WIB-Brücken. Bautechnik 2010;87(11):665–72. https://doi.org/10.1002/bate.201010044.
[22] Kouroussis G, Connolly DP, Verlinden O. Railway-induced ground vibrations – a review of vehicle effects. Int J Rail Transp 2014;2(2):69–110. https://doi.org/10.1080/23248378.2014.897791.
[23] Firus A, Berthold H, Schneider J, Grunert G. Untersuchungen zum dynamischen Verhalten einer Eisenbahnbrücke bei Anregung durch den neuen ICE 4. VDI-Berichte 2018;2321:233–48.